

One-step Electrochemically Modulated Synthesis of Reduced Graphene Oxide-Silver Nanocomposites as Efficient Nonenzymatic H₂O₂ Sensor

*Su-Juan Li**, *Jing-Chao Zhang*, *Juan Li*, *Wen-Tian Wang*, *Rui-Ting Liu*

Henan Province Key Laboratory of New Optoelectronic Functional Materials, College of Chemistry and Chemical Engineering, Anyang Normal University, Anyang, 455000, Henan, China.

*E-mail: lemontree88@163.com

Received: 13 March 2017 / *Accepted:* 29 April 2017 / *Published:* 12 May 2017

In the present work, one-step electrochemical method was utilized to synthesize reduced graphene oxide-silver nanoparticles (RGO-AgNPs) composites modified electrode. By modulating the electrodeposition potential, uniform and highly dispersed AgNPs were deposited onto RGO surface, the morphology of which was characterized by scanning electron microscopy (SEM). Electrochemical impedance spectroscopy (EIS) and cyclic voltammetry (CV) were used to investigate the electrochemical properties of this RGO-AgNPs modified electrode. When the resultant RGO-AgNPs composites were employed in fabricating a nonenzymatic H₂O₂ sensor, good electrocatalytic activity characterized with low over-potential and large current response was found for H₂O₂ reduction. The proposed sensor also exhibited excellent analytical parameters for amperometric detection of H₂O₂, such as rapid response time, wide linear range, high sensitivity and selectivity, low detection limit, acceptable reproducibility and stability. This work shows prospects for fabricating high-performance electrochemical sensors.

Keywords: Electrodeposition; Reduced graphene oxide; Ag nanoparticles; Hydrogen peroxide

1. INTRODUCTION

Hydrogen peroxide (H₂O₂) is an important intermediate of a wide range of enzymatic reactions, playing a crucial role in many fields such as biochemistry, fuel cells, pharmaceutical, food and environmental studies. The level of H₂O₂ in physiological conditions has been proved to be associated with many chronic diseases including Alzheimer's, cardiovascular and Parkinson's disease [1,2]. Therefore, it is very urgent to develop new strategies for accurate and sensitive determination of H₂O₂. Various techniques such as titrimetry [3,4], chemiluminescence [5], spectrophotometry [6] and

electrochemistry [7] have been developed. Among them, electrochemistry using modified electrode is a powerful technique due to its rapidness, cost-effectiveness, high sensitivity and selectivity, as well as suitable for in vivo analysis. Nowadays, increasing the sensitivity and improving the selectivity of modified electrode is still a challenge for monitoring of H_2O_2 in real samples.

As previously reported [8], the electrocatalytic redox kinetic of H_2O_2 at ordinary solid electrodes is slow which resulted in reduced sensitivity and poor selectivity. An effective way to speed up the electron transfer of H_2O_2 at electrodes is by introduction of enzyme [9]. Unfortunately, its application is limited due to expensive, non-selective and unstable nature of these enzyme based biosensors. An alternative method is searching for effective electrocatalyst as electrode modifications to electrocatalyze the redox reaction of H_2O_2 with high current output at low over-potential [10]. The latter strategy has attracted considerable interest, and different metals and metal oxides such as Pt [11], Pd [12], Au [13,14], Ag [15], Co_3O_4 [16], MnO_2 [17], CuO [18] nanostructures have been developed as reliable electrocatalyst to increase the detection sensitivity and selectivity of H_2O_2 .

Silver, as a noble metal, has been widely used for electrocatalytic reduction of H_2O_2 because of its extraordinary catalytic activity, biocompatibility and availability. The extraordinary catalytic activity of silver is attributed to the fact that Ag surface promotes the formation of the adsorbed OH, an intermediate of H_2O_2 reduction [19]. Ag nanostructured material with large surface to volume ratio is demonstrated especially desirable for electrocatalyzing H_2O_2 . To further improve the performance of Ag based H_2O_2 electrochemical sensor, most of this subject is by hybridization of AgNPs with highly conductive carbon nanomaterials [20,21]. Through this design, the electron transfer between H_2O_2 and electrodes is greatly enhanced, in addition, the carbon nanomaterial with large surface area is the promising matrix for stabilizing and dispersing AgNPs.

Graphene, a single sheet of two dimensional crystal carbon materials, possess unique properties such as large surface area, good electrical conductivity and chemical stability. Recently, great effort has been paid to fabricate the nanocomposites with graphene nanosheets or its derivatives and AgNPs using various techniques [22-24]. The electrochemical technique for synthesis of nanocomposites has been attracted more and more research interest, due to its direct deposition onto electrode surface without the complicated modification step. However, most of the developed electrochemical techniques involve multiple steps, including the preparation of graphene or its derivatives by reduction of graphene oxide (GO) and the subsequent electrosynthesis of AgNPs to obtain the nanocomposites [25-28], which is complex and not synchronized. Using one-step electrochemical method, reduced graphene oxide (RGO)-metal or metal oxide nanocomposites has been synthesized in our previous work [29,30]. Therefore, it is expected to be a potential technique for facile preparation of RGO-AgNPs composites.

In this work, by combining the advantages of graphene and active AgNPs, we fabricated RGO-AgNPs composites as efficient catalyst for electroreduction of H_2O_2 . By adjusting the reduction potential for preparation of nanocomposites, uniform and highly dispersed AgNPs were deposited onto surface of RGO modified electrode, and the resultant electrode shows good electrocatalytic activity toward reduction of H_2O_2 , thus an excellent performance of the present nonenzymatic H_2O_2 sensor was obtained. Therefore, the proposed one-step electrochemically modulated synthesis of RGO-AgNPs composites shows potentials in fabricating highly efficient nonenzymatic H_2O_2 sensor.

2. EXPERIMENTAL SECTION

2.1. Reagents and materials

GO was supplied by Nanjing XFNANO Materials Tech Co., Ltd. Silver nitrite (AgNO_3), H_2O_2 , glucose, ascorbic acid (AA), L-tyrosine, dopamine (DA), uric acid (UA) were obtained from Sinopharm Chemical Reagent Co., Ltd. (Shanghai, China) without the further purification. K_2HPO_4 and NaH_2PO_4 were used to prepare the supporting electrolyte of 0.1 M phosphate buffer solution (PBS, pH 7.0). Deionized water (18.2 $\text{M}\Omega$ cm) was prepared by a Milli-Q water purification system.

2.2. Apparatus

The surface morphology of synthesized modified electrode was observed from field emission scanning electron microscopy (FESEM, Hitachi SU8010, Japan). Electrochemical measurements were performed on a CHI 660D electrochemical analyzer (CHI Instruments Shanghai, China) with a conventional three-electrode system. The RGO-AgNPs composites modified glassy carbon electrode (RGO-AgNPs/GCE) was used as the working electrode, a saturated calomel electrode (SCE) as the reference electrode and a Pt wire as counter electrode.

2.3. Electrochemical preparation of RGO-AgNPs composites modified electrode

Prior to modification, a bare glassy carbon electrode (diameter of 2 mm) was carefully polished with 1.0, 0.3 and 0.05 μm alumina slurries respectively to obtain a mirror-like surface. The polished electrode was ultrasonicated in acetone, ethanol, and deionized water in sequence. Then, 10 μL 1 mg/mL GO aqueous solution was coated onto electrode surface, and allowed to dry to obtain GO modified electrode (GO/GCE). The obtained GO/GCE was subsequently immersed into deposition solutions with 5 mM AgNO_3 and 0.1 M KNO_3 involved, and a constant reduction potential of -0.6 V was kept for 120 s by using the above three-electrode system. By this method, RGO-AgNPs/GCE was successfully prepared. For comparison, the bare GCE and GO/GCE were immersed into deposition solutions of 5 mM AgNO_3 +0.1 M KNO_3 and 0.1 M KNO_3 , respectively, to prepare the AgNPs/GCE and RGO/GCE according to the same electrochemical method described above.

2.4 Electrochemical sensing of H_2O_2

The amperometric sensing of H_2O_2 was performed at an applied potential of -0.2 V by adding various aliquots of H_2O_2 stock solution into electrochemical cell with 10 mL 0.1 M PBS (pH 7.0) contained. The PBS solution was kept continuously stirred to make the concentration of added H_2O_2 uniform. Current-time curve was performed to record the steady state current response with interval of 50 s for every addition of H_2O_2 .

3. RESULTS AND DISCUSSION

3.1. Electrochemical and morphology characterization of RGO-AgNPs composites modified electrode

The current response of GO/GCE in deposition solutions with 5 mM AgNO_3 and 0.1 M KNO_3 involved at deposition potential of -0.6 V for a duration time of 120 s is shown in Fig. 1a. During this electrodeposition process, the GO was partly reduced to RGO, meanwhile, AgNPs was electrodeposited onto RGO surface to form RGO-AgNPs composites. Electrochemical impedance spectroscopy (EIS) plots are measured in $[\text{Fe}(\text{CN})_6]^{3-/4-}$ mediator for bare GCE and RGO-AgNPs/GCE to investigate impedance changes of the electrode. The charge transfer resistance of electrode is related to the diameter of semicircular part in EIS plots. As shown in Fig. 1b, the charge transfer resistance of RGO-AgNPs/GCE becomes significantly smaller than bare electrode, the results of which is similar with that described for AgNPs supported on N-doped graphene hybrid [31] and GO-Ag nanocomposites [32]. This phenomenon indicates that the modification of RGO-AgNPs composites promote the electron transfer rate of $[\text{Fe}(\text{CN})_6]^{3-/4-}$ on electrode surface, probably due to the good conductivity of RGO and Ag materials.

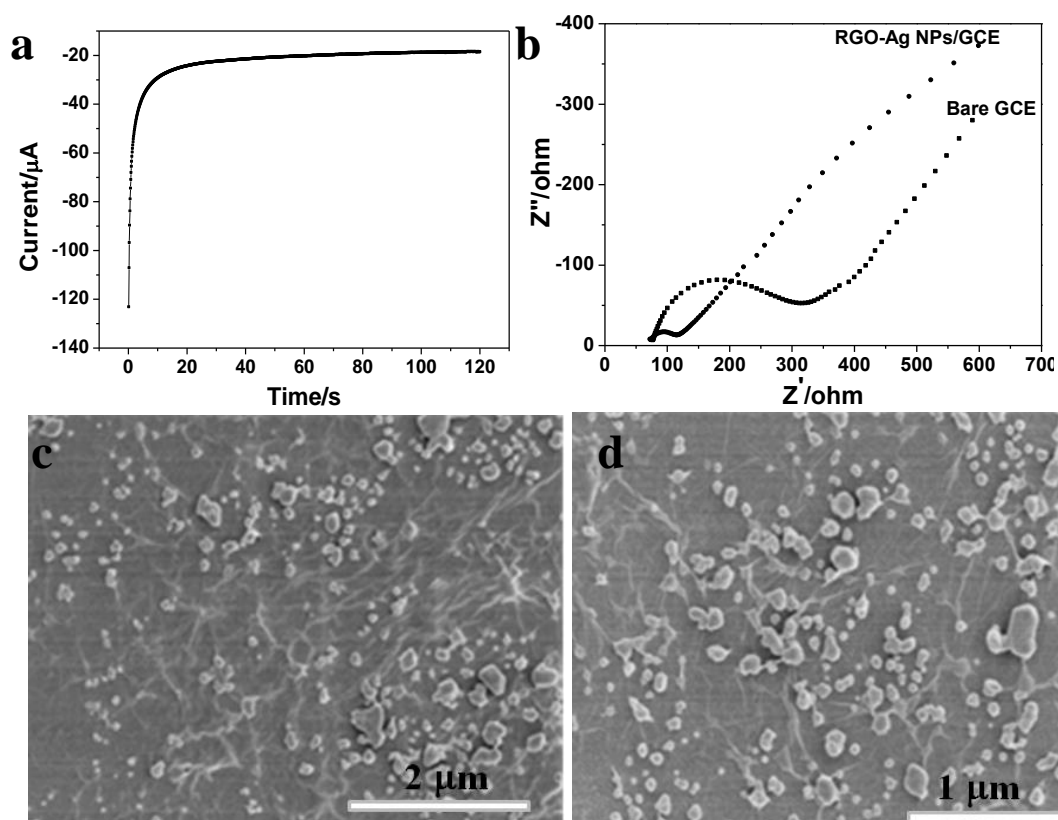


Figure 1. (a) The current response of GO/GCE in deposition solutions with 5 mM AgNO_3 and 0.1 M KNO_3 involved at deposition potential of -0.6 V for a duration time of 120 s; (b) EIS plots measured in 10 mM $[\text{Fe}(\text{CN})_6]^{3-/4-}$ +0.1 M KCl for the bare GCE and RGO-AgNPs/GCE. The frequency range of EIS was from 0.1 to 10^5 Hz at 0.2 V; (c) and (d) are the FESEM images of RGO-AgNPs/GCE prepared at deposition potential of -0.6 V for 120 s with different magnifications.

Fig. 1c and 1d show the FESEM images of the RGO-AgNPs composites synthesized according to procedures used in Fig.1a. As observed, the wrinkled and ripple-like surface of the RGO film is decorated with AgNPs with diameters ranging from 25 to 100 nm. The AgNPs is uniformly dispersed on RGO surface without obvious aggregation. In this case, the active sites of AgNPs can be fully utilized, and the resultant RGO-AgNPs composite is ideal electrocatalyst due to its large surface area. Therefore, the proposed one-step electrochemical method is feasible for preparation of highly efficient RGO-AgNPs electrocatalysts.

3.2. Effect of deposition potential for preparation of RGO-AgNPs composites on the electrochemical behavior of H_2O_2 reduction

As previously reported, the applied cathodic potentials have significant effect on reduction extent of GO [33]. With negative shift of the cathodic potential, more and more oxygenated groups can be eliminated from GO surface to form RGO. Meanwhile, once the applied potential is negative than the critical value (0.8 V vs SHE) for driving the reaction ($Ag^+ + e^- \rightarrow Ag$) to occur [34], Ag nanostructures can be deposited on electrode surface, and its morphology and structure can be modulated by the applied potentials. In order to investigate the effect of the applied potentials on the morphology of synthesized RGO-AgNPs composites, the electrodeposition was performed at potentials ranging from -0.5 to -1.2 V for a duration time of 120 s. The FESEM images are shown in Fig. 2. At a deposition potential of -0.5 V, Ag nanodendrites and aggregated AgNPs were both observed on RGO surface (Fig. 2a). However, these Ag nanostructures were distributed unevenly and only part of the RGO surface was decorated with these Ag nanostructures. At a deposition potential of -0.6 V, AgNPs with diameters of 25~100 nm are uniformly distributed on RGO surface (Fig. 1c, 1d). With further negative shift of the deposition potential to -0.8 V, about 50 nm AgNPs aggregate together on part of the RGO surface (Fig. 2b). When the deposition potential is -1.0 V, the diameter of deposited AgNPs becomes larger to about 100 nm (Fig. 2c), but stack and aggregation of AgNPs can also be observed. However, at a deposition potential of -1.2 V, about 200 nm AgNPs are obtained and they are homogeneously distributed on RGO surface. The previous work have demonstrated that Ag nanodendrites can be obtained by direct electrodeposition on ITO surfaces when the potential is made more negative than -0.5 V, and the dendrites formation mechanism is interpreted by a diffusion limited aggregation (DLA) model [34]. Nevertheless, in the present work, Ag nanodendrites were only obtained at deposition potential of -0.5 V, and with negative shift of applied potential, the main structure of AgNPs were obtained. The possible reason is attributed to the conversion of formation mechanism for Ag nanocrystals from DLA model to aggregation-controlled growth process [35].

From these results, it can also be obtained that the diameter of deposited AgNPs becomes larger and larger with the negative shift of the applied potentials, because the driving force for crystallization is sufficient resulting in more diffusion of Ag^+ toward the electrode surface. The uniform distribution of AgNPs on RGO surface was only obtained at deposition potentials of -0.6 V and -1.2 V. We can estimate that it is possibly benefited from the match energies for GO reduction and formation of nucleation from Ag^+ reduction at these potentials. In addition, the remaining oxygenated groups on RGO surface at electrodeposition potential of -0.6 V and -1.2 V is estimated to

facilitate the uniform formation of AgNPs on its surface [36,37]. However, the detailed reason for these results needs to be further investigated.

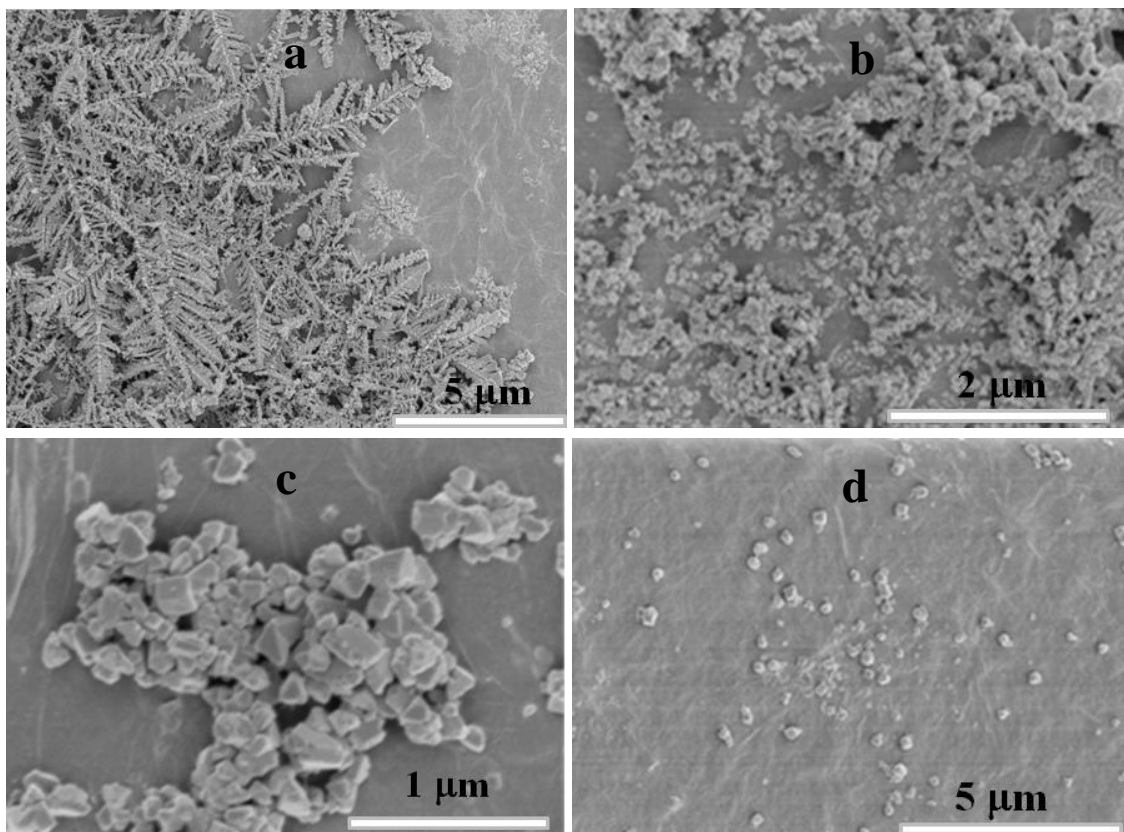


Figure 2. FESEM images of RGO-AgNPs/GCE electrodeposited at potentials of -0.5 V (a), -0.8 V (b), -1.0 V (c) and -1.2 V (d).

The morphology of nanomaterials will undoubtedly influence its electrochemical performance. Here, the effect of deposition potentials for preparation of RGO-AgNPs composites on its electrochemical behavior toward H_2O_2 reduction was investigated. The CV responses of RGO-AgNPs/GCE prepared at different reduction potentials in N_2 -saturated PBS solutions (pH 7.0) without (a) and with (b) 5 mM H_2O_2 involved are shown in Fig. 3. As can be seen from Fig. 3a, the background currents of RGO-AgNPs/GCE become larger and larger with the negative shift of deposition potentials, due to the higher surface area of RGO-AgNPs composites obtained. There is no obvious reduction peak observed in N_2 -saturated PBS solutions. However, a significant peak corresponding to reduction of H_2O_2 appears at potential of about -0.3 V at RGO-AgNPs/GCE (Fig. 3b), and the largest current response is obtained at a deposition potential of -0.6 V. The best catalytic performance of RGO-AgNPs/GCE prepared at -0.6 V is attributed to the uniform distribution of small sized AgNPs on RGO surface, which makes more catalytic sites of AgNPs exposed and enhance the effective utilization of electrocatalysts. Though a uniform distribution of AgNPs on RGO surface was also obtained at prepared potential of -1.2 V, the larger size of AgNPs makes its catalytic sites exposed limitedly, and thus a smaller reduction current compared to -0.6 V was observed. Therefore, -0.6 V

was chosen as the electrodeposition potential for preparation of RGO-AgNPs composites to construct nonenzymatic H_2O_2 sensor.

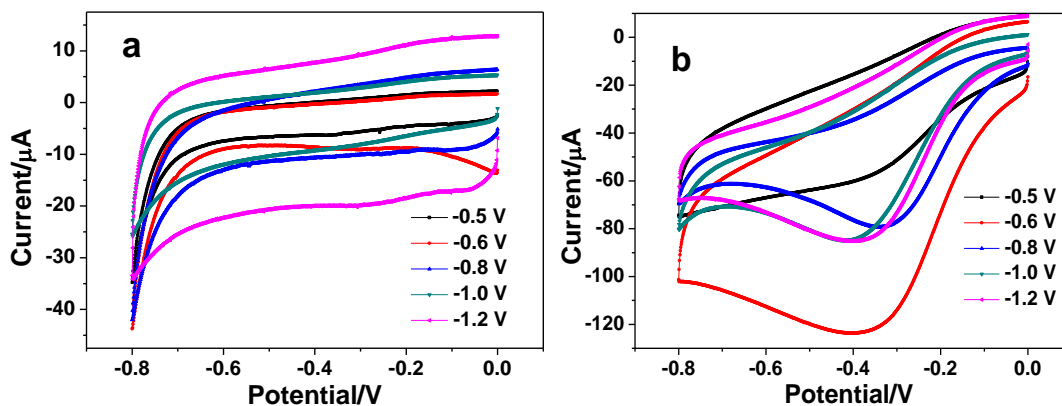


Figure 3. CV responses of the RGO-AgNPs/GCE prepared at different reduction potentials in N_2 -saturated PBS solutions (pH 7.0) without (a) and with (b) 5 mM H_2O_2 involved at a scan rate of 50 mV s^{-1} .

3.3. Electrocatalytic reduction of H_2O_2 at the RGO-AgNPs/GCE

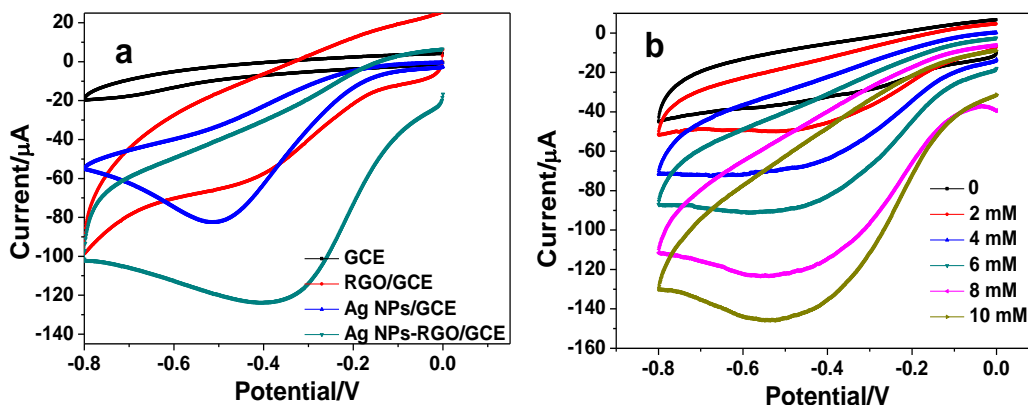


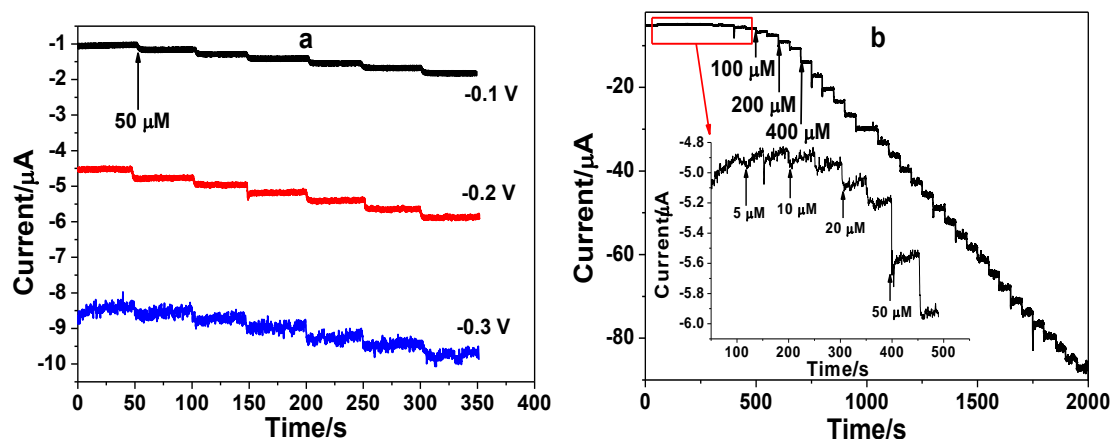
Figure 4. (a) CV responses of the bare GCE, RGO/GCE, AgNPs/GCE and RGO-AgNPs/GCE in N_2 -saturated PBS solutions (pH 7.0) with 5 mM H_2O_2 involved; (b) CV responses of RGO-AgNPs/GCE in different concentrations of H_2O_2 (0, 2, 4, 6, 8, 10 mM) at a scan rate of 50 mV s^{-1} .

To demonstrate the priority of RGO-AgNPs composites, different electrodes were studied for their electrochemical performance toward H_2O_2 reduction. Fig. 4a presents the CV responses of the bare GCE, RGO/GCE, AgNPs/GCE and RGO-AgNPs/GCE in N_2 -saturated PBS solutions (pH 7.0) with 5 mM H_2O_2 involved. It is obvious that the response of the bare GCE toward the reduction of H_2O_2 is nearly negligible. In contrast, a typical reduction peak of H_2O_2 starting from a potential of about -0.2 V was observed at the RGO/GCE and AgNPs/GCE, indicating that both RGO and AgNPs exhibit electrocatalytic effect toward reduction of H_2O_2 . When the two catalysts are integrated together

to form RGO-AgNPs composites, the RGO-AgNPs/GCE exhibits the largest reduction peak for H_2O_2 , and the onset reduction potential is at 0 V, which is more positive than RGO/GCE and AgNPs/GCE. All these observations suggest that a synergistic effect occurred for the RGO-AgNPs composites leading to excellent catalytic performance toward H_2O_2 reduction. Fig. 4b exhibits CV responses of RGO-AgNPs/GCE in different concentrations of H_2O_2 . Obviously, with the increase of H_2O_2 concentration, the reduction peak currents increase correspondingly. This result indicates that the present RGO-AgNPs composites are promising materials for constructing H_2O_2 electrochemical sensors.

3.4. Amperometric detection of hydrogen peroxide

Before amperometric detection of H_2O_2 , the applied potentials are first optimized by investigating amperometric responses of RGO-AgNPs/GCE to successive additions of $50 \mu\text{M}$ H_2O_2 at applied potentials of -0.1 , -0.2 and -0.3 V, respectively (Fig. 5a). It can be observed that the amperometric responses of $50 \mu\text{M}$ H_2O_2 at applied potentials of -0.2 and -0.3 V is larger than that of -0.1 V. However, the noise current signals at -0.3 V increase distinctly. Therefore, -0.2 V was used as the detection potential to perform quantitative analysis. Fig. 5b presents amperometric responses of the RGO-AgNPs/GCE (holding at -0.2 V) upon addition of H_2O_2 to increasing concentrations. When various concentrations of H_2O_2 were added into the stirring PBS solution, well-defined, stable and rapid current responses to the concentration of H_2O_2 were observed. The cathodic current of the sensor responded rapidly and reached 95% of the steady-state current within 3 s, showing a fast response time for amperometric detection of H_2O_2 . The calibration curve (Fig. 5c) indicates that the cathodic current increases linearly with the increase of the H_2O_2 concentration. The linear range spans the concentration range from $5 \mu\text{M}$ to 16.37 mM with the linear regression equation of $I (\mu\text{A}) = -7.76767 - 0.00703C (\mu\text{M})$ (correlation coefficient of 0.9975). The amperometric sensitivity of the sensor was calculated to be $7.03 \mu\text{A mM}^{-1}$ or $99.5 \mu\text{A mM}^{-1} \text{ cm}^{-2}$ and the limit of detection (LOD) was estimated to be $2 \mu\text{M}$ ($S/N=3$) with a signal-to-noise ratio of 3.



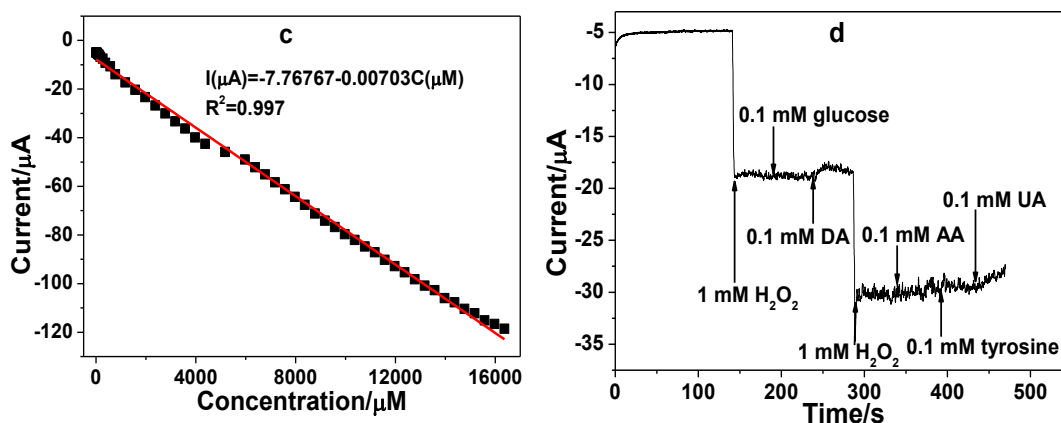


Figure 5. Amperometric detection of H_2O_2 in PBS (pH 7.0) solution using the RGO-AgNPs/GCE: (a) Amperometric responses of RGO-AgNPs/GCE to successive additions of $50 \mu\text{M}$ H_2O_2 at applied potentials of -0.1 , -0.2 and -0.3 V, respectively; (b) Amperometric responses of the RGO-AgNPs/GCE (holding at -0.2 V) upon addition of H_2O_2 to increasing concentrations; (c) The calibration curve obtained from the data of Fig. 5b; (d) Amperometric responses of the RGO-AgNPs/GCE to successive additions of 1 mM H_2O_2 , 1 mM DA, 1 mM H_2O_2 , 1 mM AA, 1 mM L-tyrosine and 1 mM UA.

To evaluate the resistant ability of the RGO-AgNPs/GCE, the influence of possible interfering substances including glucose, AA, DA, UA and L-tyrosine was examined, as shown in Fig. 5d. There is a prominently current response for the addition of 1 mM H_2O_2 . In contrast, the current responses generated by additions of 1 mM DA, 1 mM AA, 1 mM L-tyrosine and 1 mM UA can hardly be observed, indicating that the present RGO-AgNPs composites based H_2O_2 sensor has high selectivity. In addition, the reproducibility of the prepared sensor was studied by preparing six RGO-AgNPs/GCEs separately under the same conditions. The current responses of these six electrodes toward $50 \mu\text{M}$ H_2O_2 reduction yielded a relative standard deviation (RSD) of only 4.2%, which indicates an acceptable reproducibility. For one RGO-AgNPs/GCE, it was stored in room temperature for 25 days and the current was periodically measured. The current response retains 89% of its initial value after storage of 25 days. The above results demonstrated that the prepared RGO-AgNPs/GCE exhibited an excellent electrocatalytic activity, good selectivity and stability toward H_2O_2 detection.

Table 1 Comparison of RGO-AgNPs composites with various Ag based materials to hydrogen peroxide sensing.

Electrode materials	Response time (s)	Potential (V)	Sensitivity ($\mu\text{A mM}^{-1} \text{cm}^{-2}$)	Linear range (mM)	LOD (μM)	Ref.
Ag/ZIF-8/CPE	4	-0.6 vs. Ag/AgCl	398.47	0.02-5, 5.5-10	6.2	8
Hb/Ag NPs	-	-0.2 vs. Ag/AgCl	$2.83 \mu\text{A mM}^{-1}$	5×10^{-4} -20	0.42	9
3D-rGO/AgNP	-	-0.3 vs. Ag/AgCl	419.7	0.016-27	6.8	20
AgNPs/rGO	2	-0.3	-	0.1-100	3.6	22

		vs. Ag/AgCl				
ERGO–Ag	3	-0.5 vs. Ag/AgCl	-	1.6×10^{-3} -9	1.6	24
N-graphene- AgND	2	-0.4 vs. Ag/AgCl	88.47	0.1-80	0.26	27
ERGO– AgNCs	2	-0.5 vs. Ag/AgCl	183.5	0.02-10	3	28
PDA–Ag	5	-0.3 vs. SCE	$6.79 \mu\text{A mM}^{-1}$	0.092-20	1.97	38
Ag nanowire array	11-15	-0.2 vs. SCE	26.6	0.1-3.1	29.2	39
AgNP-PmPD	-	-0.9 vs. SCE	-	0.1-10	0.88	40
AuNPs/porous GaN	3	-0.6 vs. Ag/AgCl	$281.5 \mu\text{A mM}^{-1}$	0.01-0.1	2	41
GO-Ag	-	-0.3 vs. Ag/AgCl	$0.1218 \mu\text{A mM}^{-1}$	0.1-11	28.3	32
AgNPs-RGO	2	-0.3 vs. SCE	-	0.1-100	5	42
RGO-AgNPs	3	-0.2 vs. SCE	99.5 or $7.03 \mu\text{A mM}^{-1}$	5×10^{-3} -16.37	2	This work

For comparison, the performance of our present RGO-AgNPs composites with various other Ag based materials is listed in Table 1. As can be seen, the analytical parameters for amperometric detection of H_2O_2 obtained by this work including the response time, detection sensitivity, linear range and LOD are comparable and even better than those obtained by other Ag based materials. Furthermore, the detection potential used for reduction of H_2O_2 (-0.2 V) is much more positive than most of other Ag based materials [8,20,22,24,27,28,40-42], which can reduce the possible interference of reductant substances coexisting with H_2O_2 . The excellent performance of the present RGO-AgNPs composites is estimated to benefit from its good electron transfer capability with electrode, the homogeneous distribution of AgNPs on RGO surface and the synergistic effect occurred between AgNPs and RGO. Importantly, compared to other Ag based materials [25-28] prepared by multiple steps, the biggest advantage of the present sensor lies in its facile, green and simple one-step electrochemical synthesis method. All the above results suggest that the present RGO-AgNPs composites are potential electrocatalysts for catalyzing the reduction of H_2O_2 with low detection overpotential, high sensitivity and selectivity, fast response time, wide linear range, low LOD, and good stability.

4. CONCLUSIONS

In summary, homogeneous AgNPs can be electrodeposited on GO modified electrode to form RGO-AgNPs composites by modulating the cathodic deposition potentials. Due to the good electron transfer capability of nanocomposites, the morphology with homogeneous distribution of AgNPs on RGO surface and the synergistic effect occurred between AgNPs and RGO, the obtained RGO-AgNPs

composites modified electrode exhibited good electrocatalytic capability toward H₂O₂ reduction with low over-potential and large current response. When the RGO-AgNPs composites were used as nonenzymatic H₂O₂ sensors, excellent performance was obtained, including low detection potential (-0.2 vs. SCE), high sensitivity (7.03 $\mu\text{A mM}^{-1}$ or 99.5 $\mu\text{A mM}^{-1} \text{cm}^{-2}$) and good selectivity, rapid response time (within 3 s), wide linear response range (5 μM -16.37 mM) and low detection limit (2 μM), as well as acceptable reproducibility and stability. Therefore, the proposed method has potentials for fabricating efficient electrochemical sensors and biosensors.

ACKNOWLEDGEMENTS

This work was supported by the Grants from the National Natural Science Foundation of China (21105002), the fund project for Young Scholar sponsored by Henan province (14HASTIT012) and for Henan Key Technologies R&D Program (122102310516, 12B150002) and the Innovative Foundation for the College students of Anyang Normal University (ASCX/2016-Z28).

References

1. S. K. Maji, S. Sreejith, A. K. Mandal, X. Ma and Y. Zhao, *ACS Appl. Mater. Interfaces*, 6 (2014) 13648.
2. S. Chandramathi, K. Suresh, Z. B. Anita and U. R. Kuppasamy, *Parasitology*, 136 (2009) 359.
3. E. C. Hurdis and H. J. Romeyn, *Anal. Chem.*, 26 (1954) 320.
4. A. Brestovisky, E. KirowaEisner and J. Osteryoung, *Anal. Chem.*, 55 (1983) 2063.
5. Z. Lin, W. Xue, H. Chen and J. M. Lin, *Anal. Chem.*, 83 (2011) 8245.
6. P. Tanner and A. Wong, *Anal. Chim. Acta*, 370 (1998) 279.
7. X. Chen, G. Wu, Z. Cai, M. Oyama and X. Chen, *Microchim. Acta*, 181 (2013) 689.
8. A. Samadi-Maybodi, S. Ghasemi and H. Ghaffari-Rad, *Electrochim. Acta*, 163 (2015) 280.
9. L. Jiang, J. Hu and J. S. Foord, *Electrochim. Acta*, 176 (2015) 488.
10. R. Li, X. Liu, W. Qiu and M. Zhang, *Anal. Chem.*, 88 (2016) 7769.
11. L. Xing, Q. Rong and Z. Ma, *Sens. Actuators B Chem.*, 221 (2015) 242.
12. M. Han, S. Liu, J. Bao and Z. Dai, *Biosens. Bioelectron.*, 31 (2012) 151.
13. Y. Fang, S. Guo, C. Zhu, Y. Zhai and E. Wang, *Langmuir*, 26 (2010) 11277.
14. S. J. Li, Y. F. Shi, L. Liu, L. X. Song, H. Pang and J. M. Du, *Electrochim. Acta*, 85 (2012) 628.
15. X. Niu, L. Shi, J. Pan, F. Qiu, Y. Yan, H. Zhao and M. Lan, *Electrochim. Acta*, 199 (2016) 187.
16. M. Wang, X. Jiang, J. Liu, H. Guo and C. Liu, *Electrochim. Acta*, 182 (2015) 613.
17. A. J. Wang, P. P. Zhang, Y. F. Li, J. J. Feng, W. J. Dong and X. Y. Liu, *Microchim. Acta*, 175(2011) 31.
18. P. Gao, Y. Gong, N. P. Mellott and D. Liu, *Electrochim. Acta*, 173 (2015) 31.
19. G. Flatgen, S. Wasle, M. Lubke, C. Eickes, G. Radhakrishnan, K. Doblhofer and G. Ertl, *Electrochim. Acta*, 44 (1999) 4499.
20. X. Lou, C. Zhua, H. Pan, J. Ma, S. Zhu, D. Zhang and X. Jiang, *Electrochim. Acta*, 205 (2016) 70.
21. M. Baghayeri, A. Amiri and S. Farhadi, *Sens. Actuators B Chem.*, 225 (2016) 354.
22. Q. Li, X. Qin, Y. Luo, W. Lu, G. Chang, A. M. Asiri, A. O. Al-Youbi and X. Sun, *Electrochim. Acta*, 83 (2012) 283.
23. S. Liu, J. Tian, L. Wang and X. Sun, *J. Nanopart. Res.*, 13 (2011) 4539.
24. B. Zhao, Z. Liu, W. Fu and H. Yang, *Electrochem. Commun.*, 27 (2013) 1.
25. L. Wang, H. Zhu, H. Hou, Z. Zhang, X. Xiao and Y. Song, *J. Solid State Electrochem.*, 16 (2012) 1693.
26. Q. Wang and Y. Yun, *Microchim. Acta*, 180 (2013) 261.

27. M. T. Tajabadi, W. J. Basirun, F. Lorestani, R. Zakaria, S. Baradaran, Y. M. Amin, M. R. Mahmoudian, M. Rezayi and M. Sookhajian, *Electrochim. Acta*, 151 (2015) 126.
28. L. Zhong, S. Gan, X. Fu, F. Li, D. Han, L. Guo and L. Niu, *Electrochim. Acta*, 89 (2013) 222.
29. S. J. Li, Y. Xing, L. L. Hou, Z. Q. Feng, Y. Tian and J. M. Du, *Int. J. Electrochem. Sci.*, 11 (2016) 6747.
30. S. J. Li, N. Xia, X. L. Lv, M. M. Zhao, B. Q. Yuan and H. Pang, *Sens. Actuators B Chem.*, 190 (2014) 809.
31. Y. Tian, F. Wang, Y. Liu, F. Pang and X. Zhang, *Electrochim. Acta*, 146 (2014) 646.
32. A. M. Noor, M. M. Shahid, P. Rameshkumar and N. M. Huang, *Microchim. Acta*, 183 (2016) 911.
33. H. L. Guo, X. F. Wang, Q. Y. Qian, F. B. Wang and X. H. Xia, *ACS Nano*, 3 (2009) 2653.
34. R. Sivasubramanian and M. V. Sangaranarayanan, *Sens. Actuators B Chem.*, 213 (2015) 92.
35. P. Meakin, *Phys. Rev. A* 27 (1983) 604.
36. H. Gao, F. Xiao, C. C. Bun and H. Duan, *ACS Appl. Mater. Interfaces* 3 (2011) 3049.
37. S. Dong, J. Xi, Y. Wu, H. Liu, C. Fu, H. Liu and F. Xiao, *Anal. Chim. Acta*, 853 (2015) 200.
38. A. J. Wang, Q. C. Liao, J. J. Feng, Z. Z. Yan and J. R. Chen, *Electrochim. Acta*, 61 (2012) 31.
39. E. Kurowska, A. Brzózka, M. Jarosz, G. D. Sulka and M. Jaskuła, *Electrochim. Acta*, 104 (2013) 439.
40. Z. Wu, S. Yang, Z. Chen, T. Zhang, T. Guo, Z. Wang and F. Liao, *Electrochim. Acta*, 98 (2013) 104.
41. M. R. Zhang, X. Q. Chen and G. B. Pan, *Sens. Actuators B Chem.*, 240 (2017) 142.
42. A. Moradi Golsheikh, N. M. Huang, H. N. Lim, R. Zakaria and C. Y. Yin, *Carbon*, 62 (2013) 405.

© 2017 The Authors. Published by ESG (www.electrochemsci.org). This article is an open access article distributed under the terms and conditions of the Creative Commons Attribution license (<http://creativecommons.org/licenses/by/4.0/>).